GENES, CHROMOSOMES & CANCER 45:482–494 (2006)

Genomewide Screening of DNA Copy Number Changes in Chronic Myelogenous Leukemia with the Use of High-Resolution Array-Based Comparative Genomic Hybridization

Noriko Hosoya,[1,2] Masashi Sanada,[1] Yasuhito Nannya,[1] Kumi Nakazaki,[1] Lili Wang,[1] Akira Hangaishi,[1] Mineo Kurokawa,[1] Shigeru Chiba,[1,2] and Seishi Ogawa[1,3,4]*

[1]Department of Hematology and Oncology, Graduate School of Medicine, University of Tokyo, Tokyo, Japan
[2]Department of Cell Therapy and Transplantation Medicine, University of Tokyo Hospital, University of Tokyo, Tokyo, Japan
[3]Department of Regeneration Medicine for Hematopoiesis, Graduate School of Medicine, University of Tokyo, Tokyo, Japan
[4]Core Research for Evolutional Science and Technology, Japan Science and Technology Corporation, Saitama, Japan

Chronic myelogenous leukemia (CML) evolves from an indolent chronic phase (CP) characterized by the Philadelphia chromosome. Without effective therapy, it progresses to an accelerated phase (AP) and eventually to a fatal blast crisis (BC). To identify the genes involved in stage progression in CML, we performed a genomewide screening of DNA copy number changes in a total of 55 CML patients in different stages with the use of the high-resolution array-based comparative genomic hybridization (array CGH) technique. We constructed Human 1M arrays that contained 3,151 bacterial artificial chromosome (BAC) DNAs, allowing for an average resolution of 1.0 Mb across the entire genome. In addition to common chromosomal abnormalities, array CGH analysis unveiled a number of novel copy number changes. These alterations included losses in 2q26.2–q37.3, 5q23.1–q23.3, 5q31.2–q32, 7p21.3–p11.2, 7q31.1–q31.33, 8pter-p12(p11.2), 9p, and 22q13.1–q13.31 and gains in 3q26.2–q29, 6p22.3, 7p15.2–p14.3, 8p12, 8p21.3, 8p23.2, 8q24.13–q24.21, 9q, 19p13.2–p12, and 22q13.1–q13.32 and occurred at a higher frequency in AP and BC. Minimal copy number changes affecting even a single BAC locus were also identified. Our data suggests that at least a proportion of CML patients carry still-unknown cryptic genomic alterations that could affect a gene or genes of importance in the disease progression of CML. This article contains Supplementary Material available at http://www.interscience.wiley.com/jpages/1045-2257/suppmat. © 2006 Wiley-Liss, Inc.

INTRODUCTION

Chronic myelogenous leukemia (CML) is a clonal disorder originating from pluripotent hematopoietic stem cells that is characterized by the Philadelphia (Ph) chromosome generated by the t(9;22)(q34;q11) (Rowley, 1973; Melo et al., 2003). CML typically shows 3 clinical stages: the initial indolent chronic phase (CP), followed by the intermediate accelerated phase (AP), and then the terminal fatal stage, blast crisis (BC). The prognosis of patients in BC is still very poor, with a median survival of only a few months (Calabretta and Perrotti, 2004). At present, no promising curative therapeutic options are available for patients in BC. The recent development of imatinib mesylate, which selectively inhibits enhanced tyrosine kinase activity of the chimeric BCR–ABL oncoprotein generated by the Ph chromosome, produced impressive therapeutic effects on patients in CP. However, the benefits from this drug seem short-lived once patients progressed to BC (Calabretta and Perrotti, 2004). Thus, to develop new therapeutic approaches for patients in BC, it is essential to identify molecular targets of blastic transformation.

The BC stage of CML is commonly associated with nonrandom secondary chromosomal changes that, in addition to the t(9;22), include +Ph, +8, i(17q), +19, t(3;21)(q26;q22), and t(7;11)(p15;p15) (Prigogina et al., 1978; Alimena et al., 1987; Blick et al., 1987; Melo et al., 2003), or with mutations in

Supported by: Grant-in-Aid for Scientific Research on Priority Areas, Ministry of Education, Culture, Sports, Science and Technology (MEXT); Grant number: KAKENHI 17013022, Grant-in-Aid for Scientific Research, Japan Society for the Promotion of Science (JSPS); Grant number: KAKENHI 16390272, Research on Human Genome, Tissue Engineering, Health and Labour Sciences Research Grants, Ministry of Health, Labour and Welfare; Japan Health Sciences Foundation.

*Correspondence to: Seishi Ogawa, Department of Hematology and Oncology, Department of Regeneration Medicine for Hematopoiesis, Graduate School of Medicine, University of Tokyo, 7-3-1, Hongo, Bunkyo-ku, Tokyo 113-8655, Japan.
E-mail: sogawa-tky@umin.ac.jp

Received 19 October 2005; Accepted 22 November 2005
DOI 10.1002/gcc.20303
Published online 19 January 2006 in Wiley InterScience (www.interscience.wiley.com).

© 2006 Wiley-Liss, Inc.

WILEY InterScience® DISCOVER SOMETHING GREAT

the *TP53*, *CDKN2A*, *RB1*, or *RAS* genes (Ahuja et al., 1989; Kelman et al., 1989; LeMaistre et al., 1989; Feinstein et al., 1991; Nakai et al., 1992, 1994; Mitani et al., 1994; Nakai and Misawa, 1995; Sill et al., 1995; Nakamura et al., 1996; Fioretos et al., 1999; Beck et al., 2000). However, the molecular mechanisms responsible for disease progression in CML have not been fully understood. Array-based comparative genomic hybridization (array CGH) is a robust technology in which a large number of genomic clones are spotted on a glass slide and comparatively hybridized to differentially labeled tumor and reference DNA to enable high-resolution analysis of copy number changes in cancer genomes (Pinkel et al., 1998). Although the array CGH technique has been drawing increasing attention as a tool for studying alterations of genomes in various tumors (Albertson and Pinkel, 2003), it had not been applied to the analysis of patients with CML.

In the present study, to identify genes underlying stage progression in CML, we manufactured Human 1M arrays containing 3,151 bacterial artificial chromosome (BAC) DNAs and performed CGH analysis in 55 primary CML samples in different stages using these arrays. A number of previously unrecognized small cryptic genomic regions were identified.

MATERIALS AND METHODS

PATIENTS AND SAMPLES

After obtaining informed consent, bone marrow or peripheral-blood samples were obtained from 55 Japanese patients diagnosed with CML. Twenty-five of the patients were in the CP stage, 4 were in the AP stage, and 26 were in the BC stage. Clinical details are summarized in Table 1. After approval by the ethical committee at the University of Tokyo, all the samples were subjected to extraction of genomic DNA and anonymized to be used for further analysis according to the regulation of the Japanese government.

Array Fabrication

We constructed Human 1M arrays containing a subset of the FISH (fluorescence in situ hybridization) Mapped Clones V1.3 collection, which were obtained from BACPAC Resources Center (Children's Hospital Oakland Research Institute, Oakland, CA). After excluding clones missing mapping information, a total of 3,151 clones were finally selected for fabrication of Human 1M arrays (Supplementary Table 1; Supplementary material for this article can be found at http://www.interscience.wiley.com/jpages/1045-2257/suppmat), which could be used for genomewide copy number detection at an average resolution of approximately 1.0 Mb. Each BAC DNA was amplified with degenerated oligonucleotide-primed PCR (DOP-PCR) according to the protocol published by Fiegler et al. (2003), with the minor modification of an equimolar combination of DOP 1, 2, and 3 primers being used in the first PCR cycles. Amplified DNA was spotted in duplicate onto GAPS^{TM} II coated slides (Corning, International K.K., Tokyo, Japan), using an Affymetrix 419 Arrayer (Affymetrix, Santa Clara, CA). Before hybridization, array slides were briefly rehydrated over steam and immediately dried on a 75°C heat block. After being baked in a drying oven at 65°C for 3 h and UV-crosslinked at 60 mJ, the slides were rinsed with 0.2× standard saline citrate (SSC) and then with distilled water. The reactive moieties of amino-silane remaining on the glass surface were inactivated for 20 min by gently shaking arrays in a blocking solution, which was freshly prepared by dissolving 4.15 g of succinic anhydride in 245 ml of 1-methyl-2-pyrrolidinone and then adding 22.5 ml of sodium borate (1M, pH 8.0). The slides were briefly rinsed with distilled water and preserved in a desiccator at room temperature, and immediately before hybridization, they were treated in boiling water for 2 min, placed in 100% cold ethanol, and then dried by centrifugation.

DNA Labeling and Hybridization to BAC Arrays

Genomic DNA was extracted from mononuclear cells of the bone marrow or peripheral blood of normal individuals using a PUREGENE^{TM} DNA Isolation Kit (Gentra Systems, Minneapolis, MN). One microgram each of normal reference genomic (male or female) and test DNA were labeled with Cy3-dUTP and Cy5-dUTP, respectively, using a BioPrime^{R} Array CGH Genomic Labeling System (Invitrogen, Carlsbad, CA). After overnight incubation at 37°C, unincorporated nucleotides were removed by use of a BioPrime^{TM} Array CGH Purification Module (Invitrogen, Carlsbad, CA). The labeled test and reference DNA were ethanol-precipitated together with 80 μg of human Cot-1 DNA (Invitrogen, Carlsbad, CA) and 100 μg of yeast tRNA (Roche, Basel, Switzerland), redissolved in a hybridization mix [50% formamide, 5% dextran sulfate, 2× SSC, 5% Tris (pH 7.4), 0.1% Tween 20], and denatured at 75°C for 15 min. After incubation at 37°C for 30 min, the mixture was

TABLE 1. Patient Characteristics, Cytogenetic Description of Their Karyotypes, and Presence of *BCR/ABL* Confirmed by FISH or RT-PCR

Case No.	Sex	Age	Stage	Phenotype	Blast(%)	Karyotype	Methods of *BCR/ABL* detection
AP1	M	51	CML AP		6	46,XY,t(9;22)(q34;q11)(20/20)	NS
AP2	F	56	CML AP		2	50,XX,t(9;22)(q34;q11)+13, +19,+21,+22(8/15) 51,XX,t(9;22)(q34;q11), +t(9;22),+13,+19,+21, +22(4/15) 52,XX,+8,t(9;22)(q34;q11), +t(9;22),+13,+19,+21, +22(2/15) 47,XX,t(9;22)(q34;q11), +19,−20,−21,+der(22) t(9;22),+mar(1/15)	FISH and RT-PCR
AP3	M	37	CML AP		3.3	46,XY,t(9;22)(q34;q11)(18/20) 47,XY,+8,t(9;22)(q34;q11) (2/20)	RT-PCR
AP4	M	74	CML AP		9	46,XY,t(9;22)(q34;q11)(14/20) 45,XY,−21,t(9;22)(q34;q11) (5/20) 45,XY,−17,t(9;22)(q34;q11) (1/20)	RT-PCR
BC1	M	78	CML BC	ND	30	46,XY,t(9;22)(q34;q11)	NS
BC2	M		CML BC	ND	72	46,XY,t(9;22)(q34;q12)	NS
BC3	M	65	CML BC	lymphoid	90	46,XY,t(9;22)(q34;q11)	NS
BC4	M	33	CML BC	lymphoid	70	NA	NS
BC5	M		CML BC	lymphoid	65	NA	NS
BC6	F	48	CML BC	lymphoid	56	46,XX,t(9;22)(q34;q11)	NS
BC7	F	42	CML BC	lymphoid	60	46,XX,t(9;22)(q34;q11)	NS
BC8	F	42	CML BC	lymphoid	70	46,XX,t(9;22)(q34;q11)	NS
BC9	F	60	CML BC	myeloid	98	46,XX,t(9;22)(q34;q11)	NS
BC10	M	62	CML BC	myeloid	90	46,XY,t(9;22)(q34;q11)	NS
BC11	F		CML BC	myeloid	60	NA	NS
BC12	F	53	CML BC	myeloid	20	NA	NS
BC13	F		CML BC	myeloid	88	NA	NS
BC14	M		CML BC	myeloid	75	NA	NS
BC15	M	46	CML BC	myeloid	70	46,XY,t(9;22)(q34;q11)	NS
BC16	M	67	CML BC	myeloid	73	48,XY,t(3;21;18)(q21;q22;p11), +8,t(9;22)(q34;q11), +12(20/20)	FISH and RT-PCR
BC17	F	57	CML BC	myeloid	39	46,XY,t(9;22)(q34;q11)(10/10)	NS
BC18	M	51	CML BC	myeloid	86	46,XY,t(9;22)(q34;q11)(20/20)	FISH and RT-PCR

(Continued)

TABLE 1. Patient Characteristics, Cytogenetic Description of Their Karyotypes, and Presence of *BCR/ABL* Confirmed by FISH or RT-PCR (Continued)

Case No.	Sex	Age	Stage	Phenotype	Blast(%)	Karyotype	Methods of *BCR/ABL* detection
BC19	M	54	CML BC	myeloid	13	NA	FISH and RT-PCR
BC20	M	69	CML BC	myeloid	35	46,XY,t(9;22)(q34;q11)(13/20) 46,XY,t(9;22)(q34;q11),der(12)t(1;12)(q12;q24)(3/20) 46,XY,t(9;22)(q34;q11),der(19)t(1;19)(q12;p13)(4/20)	FISH and RT-PCR
BC21	M	71	CML BC	lymphoid	59	48,XY,11q+,+19,22q−,+22q−(20/20)	RT-PCR
BC22	M	62	CML BC	myeloid	61	46,XY,t(20;22)(p13;q11)(8/20) 47,XY,t(20;22)(p13;q11),+der(22)t(20;22)(p13;q11)(5/20) 45,XY,del(4)(q31),add(6)(p21),der(8;17)(q10;q10),+i(8)(q10),+add(9)(p22),−13,−16,t(20;22)(p13;q11),der(22)t(20;22),inc(1/20) 44,X,−Y,add(6)(p21),der(8;17)(q10;q10),+i(8)(q10),add(9)(p22),−13,−16,t(20;22)(p13;q11),inc(1/20) 74–87, ND, including add(6)(p21),der(8;17)(q10;q10),add(9)(p22),t(20:22)(p13;q11)(5/20)	RT-PCR
BC23	M	28	CML BC	myeloid	36	46,XY,t(9;22)(q34;q11)(18/20) 46,XY(2/20)	FISH and RT-PCR
BC24	M	60	CML BC	myeloid	44	48,XY,+8,t(9;22)(q34;q11),+der(22)t(9;22)(q34;q11)(19/20) 50,XY,+8,+8,t(9;22)(q34;q11),+21,+der(22)t(9;22)(q34;q11)(1/20)	FISH and RT-PCR
BC25	M	37	CML BC	myeloid	28	46,XY,t(9;22)(q34;q11)(12/20) 46,XY(8/20)	FISH and RT-PCR
BC26	M	64	CML BC	myeloid	85	45,XY,add(5)(q15),der(9)t(9;22)(q34;q11),add(12)(p11),del(17)(p11),add(19)(q13),−21,der(22)add(22)(p11)t(9;22)(17/20)	FISH and RT-PCR

(Continued)

TABLE 1. Patient Characteristics, Cytogenetic Description of Their Karyotypes, and Presence of *BCR/ABL* Confirmed by FISH or RT-PCR (Continued)

Case No.	Sex	Age	Stage	Phenotype	Blast(%)	Karyotype	Methods of *BCR/ABL* detection
						45,XY,der(5)t(5;21)(q31;q11), der(9)t(9;22)(q34;q11), del(17)(p11),add(19)(q13), −21,der(22)add(22)(p11) t(9;22)(1/20) 48,XY,dup(3)(q21q27),add(4) (q21),der(5)t(5;21)(q31;q11), t(9;22)(q34;q11),add(13)(p11), del(17)(p11),+19,−21, +der(22)t(9;22),+mar(1/20) 48,XY,dup(3)(q21q27),−4, der(5)t(5;21)(q31;q11), t(9;22)(q34;q11),add(13)(p11), del(17)(p11),+19,−21, +der(22)t(9;22),+mar(1/20)	
CP1	M	40	CML CP		0	46,XY,t(9;22)(q34;q11)	NS
CP2	M	28	CML CP		0	NA	NS
CP3	F	60	CML CP		0	46,XX,t(9;22)(q34;q11)	NS
CP4	M	62	CML CP		0	46,XY,t(9;22)(q34;q11)	NS
CP5	M	38	CML CP		5	46,XY,t(9;22)(q34;q11)	NS
CP6	M	35	CML CP		5	46,XY,t(9;22)(q34;q11)	NS
CP7	M	54	CML CP		0	46,XY,t(9;22)(q34:q11)	NS
CP8	F		CML CP		0	NA	NS
CP9	M		CML CP		0	46,XY,t(9;22)(q34;q11)	NS
CP10	M		CML CP		1	46,XY,t(9;22)(q34;q11)	NS
CP11	F	32	CML CP		0	46,XX,t(9;22)(q34;q11)	NS
CP12	F	59	CML CP		0	46,XX,t(9;22)(q34;q11)	NS
CP13	M	51	CML CP		0	46,XY,t(9;22)(q34;q11)	NS
CP14	F		CML CP		0	46,XX,t(9;22)(q34;q11)	NS
CP15	M	46	CML CP		0	46,XY,t(9;22)(q34;q11)	NS
CP16	M	58	CML CP		0	46,XY,t(9;22)(q34;q11)	NS
CP17	F	58	CML CP		0	46,XX,t(9;22)(q34;q11)	NS
CP18	F	74	CML CP		0	46,XX,t(9;22)(q34;q11)	NS
CP19	F	54	CML CP		0	46,XX,t(9;22)(q34;q11)	NS
CP20	M		CML CP		0.5	46,XY,t(9;22)(q34;q11)	NS
CP21	M	71	CML CP		0	46,XY,t(9;22)(q34;q11)(20/20)	NS
CP22	M	40	CML CP		0	46,XY,t(9;22)(q34;q11)(20/20)	FISH and RT-PCR
CP23	M	43	CML CP		1.5	46,XY(20/20)	FISH and RT-PCR
CP24	F	55	CML CP		2	46,XX,t(9;22)(q34;q11)(20/20)	NS
CP25	M	75	CML CP		0	46,XY,t(9;22)(q34;q11)	NS

ND: not determined; NA: information not available; NE: not examined; NS: not specified in clinical records; Ph chr: Philadelphia chromosome; chr: chromosome; RT-PCR: reverse-transcriptase-polymerase-chain-reaction; The t(20;22)(p13;q11) in case BC26 is a variant Ph translocation.

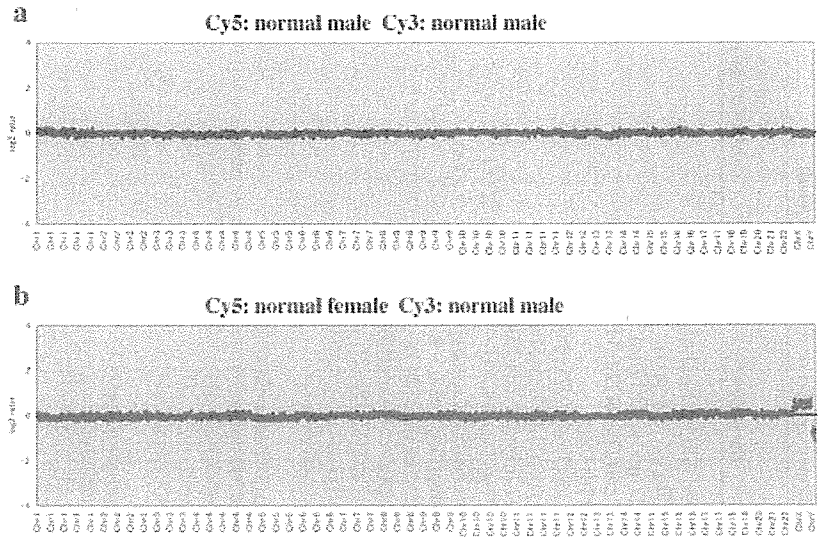

Figure 1. Representative array CGH results obtained from reference-versus-reference control hybridization. Clones are ordered from chromosomes 1 to 22, X, and Y and within each chromosome according to the UCSC mapping position (http://genome.ucsc.edu/; May 2004 draft). Each spot represents an average $\log_2$ signal ratio for each BAC locus. (a) For all loci, $\log_2$ ratios were within the thresholds −0.2 and 0.2 in the male-versus-male control experiment. (b) Gain in chromosome X (0.435 ± 0.124) and loss in chromosome Y (−0.807 ± 0.167) were clearly visualized in the female-versus-male control experiment (Cy5 and Cy3, respectively).

applied to an array slide placed in a MAUI® Mixer AO Hybridization Chamber Lid (BioMicro Systems, Salt Lake City, UT) and incubated at 37°C for 60–66 h using a MAUI Hybridization System (BioMicro Systems). After hybridization, the slides were washed once in a solution of 50% formamide and 2× SSC for 15 min at 50°C and once in 2× SSC for 15 min at room temperature. Slides were rinsed briefly with 0.2× SSC and dried immediately by centrifugation.

Image Analysis and Processing

After hybridization, the arrays were scanned by an Affymetrix 428® Array Scanner (Affymetrix, Santa Clara, CA). The scanned image was analyzed by an ImaGene v4.2 (BioDiscovery, Inc., Marina Del Rey, CA) in order to extract Cy3 and Cy5 signals for each spot, and after local background signals were subtracted, test/reference $\log_2$ ratios of the test and reference signals were calculated for all spots. The $\log_2$ ratios were normalized so that the average $\log_2$ ratio of all spots became zero. A spot was eliminated from the analysis if the signal intensity after the background subtraction in either Cy5 or Cy3 was less than −18 decibels or the duplicated signals differed by more than 0.4 in the $\log_2$ ratios. The average $\log_2$ ratios of the two replicate spots were calculated for the remaining spots. An experiment was not adopted if less than 90% of all spots met the above-mentioned criteria or if the standard deviation (SD) of all spots was larger than 0.25. Thresholds for copy number gain and loss were defined as $\log_2$ ratios of +2 SD and −2 SD, respectively. The reproducibility of the data was confirmed in two independent experiments for each tumor sample. For two representative cases, the consistency of the CGH results was confirmed by dye-swap experiments, in which tumor and reference DNA were inversely labeled with Cy3 and Cy5, respectively.

FISH Analysis

Interphase FISH experiments were performed as previously described (Wang et al., 2003).

RESULTS

Quality Test of BAC Array

Prior to the analysis of CML samples, control experiments were performed to evaluate the quality of the Human 1M array, in which DNA from normal individuals was used as a test sample. In the male-versus-male control hybridizations, $\log_2$ ratios for all spots were within the thresholds of −0.2 and 0.2 (Fig. 1a), whereas in the female-versus-male hybridizations, copy number gain of the whole chromosome X and copy number loss of the whole chromosome Y were detected successfully (Fig. 1b). In the latter experiments, the mean $\log_2$ ratios of the clones on the X and Y chromosomes were 0.435 ± 0.124 and −0.807 ± 0.167, respectively, compared to the mean $\log_2$ ratio of −0.008 ± 0.083 for all clones from autosomal chromosomes.

Higher Frequency of DNA Copy Number Changes in CML in BC and AP

A total of 55 CML samples in different stages were analyzed for copy number alterations by array CGH using Human 1M arrays. Table 2 lists the copy number alterations detected in individual

TABLE 2. Gains and Losses Detected by Array CGH

Case No.	Regions and clones that showed copy number gains	Regions and clones that showed copy number losses
AP1	3q26.2–q29 (RP11-91A17~RP11-233N20), 7p15.2–p14.3 (RP11-81F15~RP11-89N17)	22q13.2–q13.31 (RP11-81N15~RP11-66M5)
AP2	9p21.2 (RP11-81B19)-qter, Chromosome13, Chromosome19, Chromosome21, Chromosome22, ***22q11.1–q11.22*** **and** ***9q34.13–qter*** 22q13.1–q13.32 (RP11-4H24-RP11-133P21)	**8p23.1 (RP11-287P18)**
AP3	**5p15.1 (RP11-88L18, RP11-90B23), 19p13.2 (RP11-79F15)**	none
AP4	**8q21.2 (RP11-90G23)**	none
BC1	none	none
BC2	none	none
BC3	**4p15.33 (RP11-143I20), 5p15.1 (RP11-88L18)** 8p12 (RP11-274F14-RP11-100B16), 9q, **19p13.2 (RP11-79F15),** ***22q11.1–q11.22 and 9q34.13–qter***	**1q25.1 (RP11-177M16),** 5q23.1–q23.3 (RP11-47L19-RP11-89G4), 5q31.2–q32 (RP11-11514~RP11-88H2), 7q31.1–q31.33 (RP11-79G19~RP11-90C13), 8pter–p12 (RP11-91P13), 9p
BC4	**8p23.1 (RP11-287P18), 22q11.21 (RP11-278E23)**	none
BC5	**8p23.1 (RP11-287P18), 17p13.3 (RP11-582C6), 19p13.2 (RP11-79F15)**	**17q21.31 (RP11-52N13)**
BC6	none	**5p15.1 (RP11-88L18)**
BC7	Chromosome8	none
BC8	none	none
BC9	none	**21q22.12 (RP11-17O20)**
BC10	**8p23.1 (RP11-287P18), 17p13.3 (RP11-582C6)**	none
BC11	none	none
BC12	**8p23.1 (RP11-287P18), 17p13.3 (RP11-582C6)**	**5p15.1 (RP11-88L18)**
BC13	none	Chromosomes 4 and 13
BC14	Chromosome8, **8q21.2 (RP11-90G23)**	none
BC15	**8p23.1 (RP11-287P18)**	none
BC16	Chromosome8*, **8p23.1 (RP11-287P18),** Chromosome12*, **17p13.3 (RP11-582C6),** ***22q11.1–q11.2 and 9q34.13–qter***	2q36.2–q37.3 (RP11-68H19~RP11-90E11*), 18pter–q11.2 (RP11-79F3)*
BC17	none	**1q25.3 (RP11-196B7), 17q21.31 (RP11-52N13)**
BC18	none	**1q25.3 (RP11-173E24), 1q25.3–q31.1 (RP11-162L13)**
BC19	none	**5p15.1 (RP11-88L18),** 7p21.3–p11.2 (RP11-79O21~RP11-90N11)
BC20	none	**9q22.32 (RP11-223A21)**
BC21	**5p15.1 (RP11-88L18),** Chromosome19*, ***22q11.1–q11.2 and 9q34.13–qter***	none
BC22	6p22.3 (RP11-43B4~RP11-288M24), 8p21.3 (RP11-89O4~RP11-274M9), 8p11.21 (RP11-282J24)-qter	8pter–p11.2 (RP11-284J3)
BC23	**5p15.1 (RP11-88L18)**	none
BC24	Chromosome8*, **17p13.3 (RP11-582C6), 17q22 (RP11-143M4)** ***22q11.1–q11.2 and 9q34.13–qter***	**5p15.1 (RP11-88L18), 7q11.21 (RP11-90C3)**
BC25	**5p15.1 (RP11-88L18), 19p13.2 (RP11-79F15)**	none
BC26	8q24.13–q24.21 (RP11-229L23-RP11-237F24), 19p13.2–p12 (RP11-84C17~RP11-91L5), ***22q11.1–q11.2 and 9q34.13–qter***	none
CP1	**8p23.1 (RP11-287P18), 17p13.3 (RP11-582C6)**	**1q25.1 (RP11-177M16), 1q25.3 (RP11-173E24), 5p15.1 (RP11-88L18)**
CP2	**17q21.31 (RP11-52N13)**	**1q25.1 (RP11-177M16)**
CP3	**17p13.3 (RP11-582C6), 17q12(CTD-2019C10)**	**5p15.1 (RP11-88L18), 17q25.2 (RP11-145C11)**

(Continued)

TABLE 2. Gains and Losses Detected by Array CGH (Continued)

Case No.	Regions and clones that showed copy number gains	Regions and clones that showed copy number losses
CP4	**5p15.1 (RP11-88L18), 19p13.2 (RP11-79F15)**	**1q25.1 (RP11-177M16), 17q21.31 (RP11-52N13)**
CP5	none	none
CP6	none	**5p15.1 (RP11-88L18)**
CP7	**19p13.2 (RP11-79F15)**	none
CP8	none	Chromosome3
CP9	none	none
CP10	none	none
CP11	none	none
CP12	**6q25.3–q26 (RP11-43B19)**	none
CP13	**8p23.1 (RP11-287P18), 17p13.3 (RP11-582C6)**	none
CP14	**19p13.2 (RP11-79F15)**	none
CP15	8p23.2 (RP11-113B7~RP11-89I12), **8p23.1 (RP11-287P18), *22q11.1–q11.2 and 9q34.13–qter***	none
CP16	**19p13.2 (RP11-79F15)**	**8q21.2 (RP11-90G23)**
CP17	none	none
CP18	**17p13.3 (RP11-582C6)**, 17p11.2–qter	**17q12(CTD-2019C10)** 17pter–p12
CP19	none	none
CP20	**19p13.2 (RP11-79F15)**	**5p15.1 (RP11-88L18)**
CP21	**8p23.1 (RP11-287P18), 15q22.31 (RP11-50N10), 22q13.32 (RP11-133P21)**	**1q25.1 (RP11-177M16)**
CP22	none	none
CP23	none	none
CP24	none	**5p15.1 (RP11-88L18, RP11-90B23), 8q21.3 (RP11-91K2), 9q32 (RP11-95J4)**
CP25	none	none

22q11.1–11.2 and ***9q34.13–qter*** corresponds to Philadelphia chromosome.
Gain of 17p11.2–qter together with loss of 17pter–p12 represents isochromosome 17q (i(17q)).
Copy number changes involving a single BAC are indicated in bold. Underlined are the regions (or BAC loci) whose copy number changes were confirmed by FISH.

cases, and Table 3 summarizes the number of cases showing each copy number alteration in different stages of CML. Array CGH successfully detected cryptic gains and losses that had been missed by conventional karyotyping analysis as well as large chromosomal changes that had been observed in prior conventional karyotyping analysis (Tables 2 and 3).

When analysis was confined to copy number alterations that involved at least two consecutive BAC clones, only 4 copy number alterations were detected in 25 patients in CP, whereas 38 copy number alterations were identified in 30 patients in AP/BC (Table 2). The frequency of DNA copy number alterations was significantly higher in AP/BC than in CP ($P < 0.005$).

Large and Small Cryptic Changes Detected by High-Resolution Array CGH

In the current analysis, the most frequent alteration was gain of extra Ph chromosomes (6 cases in AP/BC, 1 case in CP), which was inferred from gains of a distal part of 9q and a proximal part of 22q. Alterations of whole chromosomes, including gains of chromosomes 8 (4 cases in BC), 19 (2 cases in AP/BC), 13, 21, and 22 (1 case each in AP), and losses of chromosomes 3 (1 case in CP), 4, and 13 (1 case each in BC) were also observed (Tables 2 and 3). One CP patient (case CP18) displayed both gain of 17p11.2–qter and loss of 17pter–p12 material, suggesting the presence of an isochromosome 17q—i(17q)—which has repeatedly been reported in association with CML BC (Prigogina et al., 1978; Alimena et al., 1987; Fioretos et al., 1999; Melo et al., 2003), although the conventional karyotyping analysis had missed this abnormality.

Our array CGH analysis also uncovered cryptic changes that had not been reported in CML and therefore were novel regions implicated in the pathogenesis and progression of CML. Case BC3 was found to have a balanced t(9;22) translocation as the sole chromosomal abnormality in karyotyp-

TABLE 3. Summary of Copy Number Alterations Detected by Array CGH

	Stage	
	CP ($n = 25$)	AP + BC ($n = 30$)
Gains		
Unbalanced translocations or gains that were also detected by G-banding analysis		
Ph (22q11.1–q11.2 and 9q34.13–qter)	0	3
Chromosome 8	0	2
Chromosome 13	0	1
Chromosome 19	0	2
Chromosome 21	0	1
Chromosome 22	0	1
Gains in cases in which G-banding analysis was not done		
Chromosome 8	0	1
3q26.2–q29	0	1
7p15.2–p14.3	0	1
8p11.21–q24.3	0	1
Cryptic gains that were not detected by G-banding analysis (involving at least two consecutive BAC clones spotted on the array)		
Ph (22q11.1–q11.2 and 9q34.13–qter)	1	3
i(17q) (gain of 17p11.2–qter and loss of 17pter–p12)	1	0
Chromosome 8	0	1
6p22.3	0	1
8p12	0	1
8p21.3	0	1
8p23.2	1	0
8q24.13–q24.21	0	1
9p21.2–qter	0	1
9q	0	1
19p13.2–p12	0	1
22q13.1–q13.32	0	z1
Total number	3	26
Losses		
Losses in cases in which G-banding analysis was not done		
Chromosome 3	1	0
Chromosome 4	0	1
Chromosome 13	0	1
7p21.3–p11.2	0	1
22q13.1–q13.31	0	1
Cryptic losses that were not detected by G-banding analysis (involving at least two consecutive BAC clones spotted on the array)		
2q36.2–q37.3	0	1
5q23.1–q23.3	0	1
5q31.2–q32	0	1
7q31.1–q31.33	0	1
8pter–p12	0	1
8pter–p11.2	0	1
9p	0	1
18pter–q11.2	0	1
Total number	1	12

ing analysis (Tables 1 and 2). However, in array CGH, multiple copy number alterations, including gains in 8p12 and 9q, and an extra Ph chromosome, and losses in 5q23.1–q23.3, 5q31.2–q32, 7q31.1–q31.33, 8pter–p12, and 9p were reproducibly detected in duplicate experiments (Table 2, Fig. 2a). Case BC16 had a karyotype showing 48,XY, t(3;21;18)(q21;q22;p11),+8, t(9;22)(q34;q11), +12 (Table 1), whereas array CGH also detected an extra Ph chromosome as well as losses in 2q36.2–q37.3 and 18pter–q11.2 (Table 2, Fig. 2b). Also, in case BC22, CGH analysis disclosed cryptic copy number gains in three consecutive BACs within a small 6p22.3 region spanning 505 kb (Table 2, Fig. 2c).

These array CGH results were confirmed by FISH analysis using affected BAC clones as probes when Carnoy samples were available (Table 2, Fig. 2b and c). For example, the sample from patient BC16 showed, consistent with trisomies 8 and 12, three signals from clones RP11-150N13, on chromosome 8 (with an average $\log_2$ ratio of 0.449), and RP11-91I15, on chromosome 12 (with an average $\log_2$ ratio of 0.474), whereas clones RP11-116M19, on chromosome 2 (with an average $\log_2$ ratio of −0.538), and RP11-105C15, on chromosome 18 (with an average $\log_2$ ratio of −0.701), produced only one signal, confirming the presence of an allelic deletion in these regions (Fig. 2b). In patient BC22, clones RP11-228M24, at 6p22.3 (with an average $\log_2$ ratio of 1.158), showed multiple signals, in agreement with the copy number gain found in array CGH (Fig. 2c).

Copy number changes that involved only a single BAC locus (Table 4) were verified by FISH analysis for selected cases (Table 2 and Fig. 2d). In total, 75 single BAC copy number changes (SBCs) were identified in 24 BAC loci among 55 CML patients. Because 35 of the 75 SBCs, found in three BAC loci, were also identified in normal individuals (3 SBCs, at RP11-88L18, RP11-287P18, and RP11-586C6, in 10 healthy Japanese individuals; data not shown) and 37 SBCs in six BAC loci appeared as both copy number gains and losses depending on samples, suggesting that many of these are likely to represent polymorphisms known as large-scale copy number variations (LCVs; Iafrate et al., 2004; Sebat et al., 2004; Table 4). Indeed, 11 of the 24 BAC loci showing SBCs conformed to regions previously reported as LCVs (Table 4) (Iafrate et al., 2004; Sebat et al., 2004).

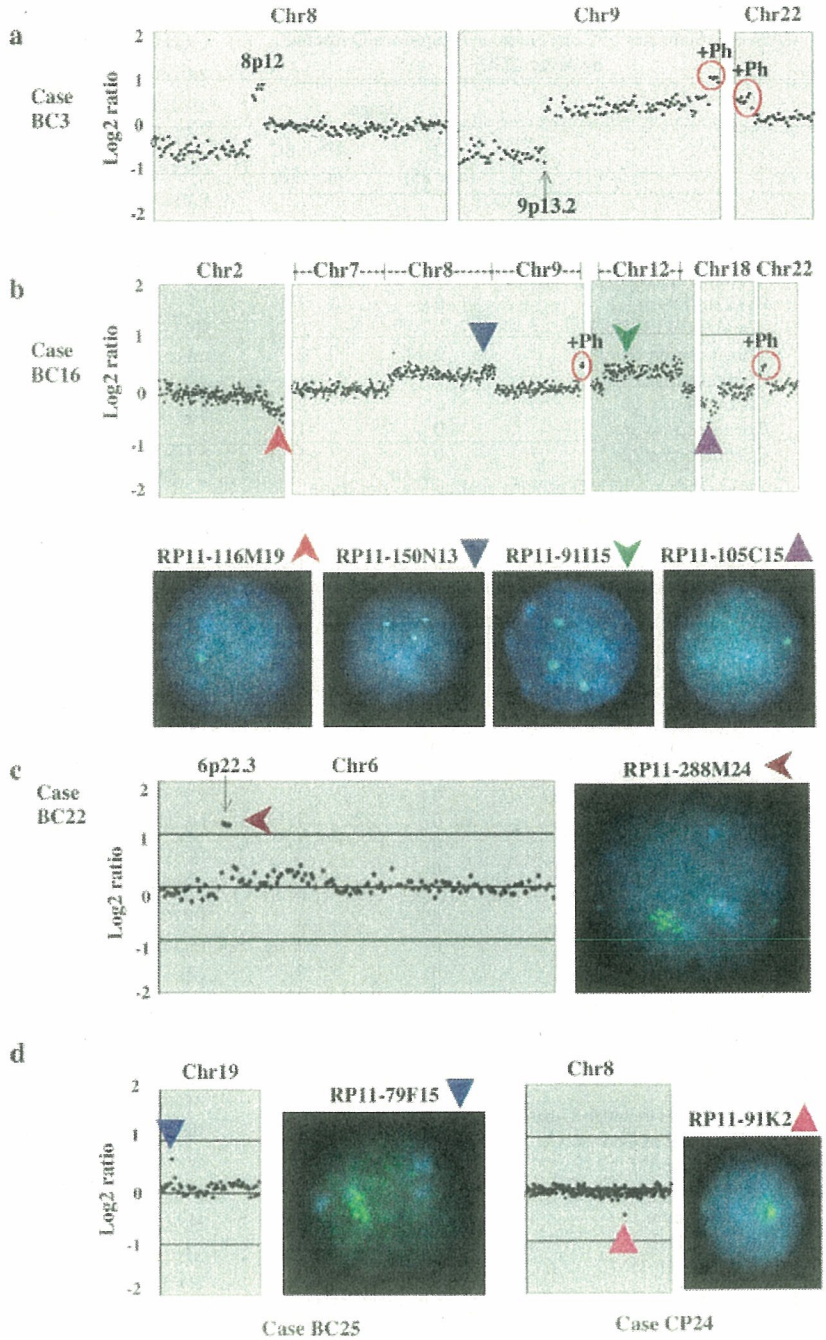

Figure 2. Gains and losses detected by array CGH and confirmed by FISH analysis. (a) Array CGH profile of case BC3, showing an extra Ph chromosome, gains in 8p12 and 9q and losses in 8pter–8p12 and 9p, not detected by karyotyping analysis; (b) Array CGH profile of case BC16, in which an extra Ph chromosome, gain in chromosome 8 with a higher-level of gain of the clone RP11-287P18, gain in chromosome 12, and losses in 2q36.2–2q37.3 and 18pter–18q11.2 were identified. Interphase FISH analysis of this case used the indicated biotin-labeled BAC clones as probes. Consistent with trisomies 8 and 12, clones RP11-150N13, on chromosome 8 (average $\log_2$ ratio of 0.449), and RP11-91115, on chromosome 12 (average $\log_2$ ratio of 0.474), showed 3 signals, whereas clones RP11-116M19, on chromosome 2 (average $\log_2$ ratio of −0.538), and RP11-105C15, on chromosome 18 (average $\log_2$ ratio of −0.701), produced only one signal, confirming an allelic deletion in these regions. (c) Array CGH profile of case BC22, for which clone RP11-288M24, at chromosome 6p22.3 (average $\log_2$ ratio of 1.158), showed multiple signals, confirming copy number gains in this region. (d) Array CGH profiles of cases BC25 and CP24, in which single BAC copy number changes were observed. Copy number gain (RP11-79F15) and loss (RP11-91K2) were verified by FISH analysis.

Candidate Genes Implicated in Pathogenesis or Disease Progression of CML

The regions showing gain or loss in DNA copy number or breakpoint regions of unbalanced chromosomal translocations could harbor one or more genes implicated in the pathogenesis of CML or disease progression to BC. Supplementary Table 2 lists the representative genes within these regions identified in this study, not including the single BAC regions showing both gains and losses. Among previously reported cellular oncogenes or leukemia-related genes were *EVI1* (3q26), *FGFR1* (8p12), and *MYC* (8q24), which were included in the regions showing copy number gains in 3q26.2–q29, 8p12, and 8q24.13–q24.21, respectively (Supplementary Table 2). The 505-kb region showing

TABLE 4. Copy Number Alterations Involving a Single BAC Locus

	Stage	
	CP ($n = 25$)	AP + BC ($n = 30$)
Gains		
4p15.33 (RP11-143I20)[a]	0	1
5p15.1 (RP11-88L18)[a]	1	5
5p15.1 (RP11-90B23)	0	1
6q25.3–q26 (RP11-43B19)[a]	1	0
8p23.1 (RP11-287P18)[a]	4	6
8q21.2 (RP11-90G23)[a]	0	2
15q22.31 (RP11-50N10)	1	0
17p13.3 (RP11-582C6)[a]	4	5
17q12 (CTD-2019C10)	1	0
17q21.31 (RP11-52N13)	1	0
17q22 (RP11-143M4)	0	1
19p13.2 (RP11-79F15)[a]	4	4
22q11.21 (RP11-278E23)[a]	0	1
22q13.32 (RP11-133P21)	1	0
Losses		
1q25.1 (RP11-177M16)	4	1
1q25.3 (RP11-196B7)	0	1
1q25.3 (RP11-173E24)	1	1
1q25.3–q31.1 (RP11-162L13)	0	1
5p15.1 (RP11-88L18)[a]	5	4
5p15.1 (RP11-90B23)	1	0
7q11.21 (RP11-90C3)[a]	0	1
8p23.1 (RP11-287P18)[a]	0	1
8q21.2 (RP11-90G23)[a]	1	0
8q21.3 (RP11-91K2)[a]	1	0
9q32 (RP11-95J4)[a]	1	0
9q22.32 (RP11-223A21)	0	1
17q12 (CTD-2019C10)	1	0
17q21.31 (RP11-52N13)	1	2
17q25.2 (RP11-145C11)	1	0
21q22.12 (RP11-17O20)	0	1

Shaded areas point to the loci that showed both gains and losses in different samples.

[a]Regions previously reported to show large-scale copy number variations (LCVs).

copy number gain at the chromosome band 6p22.3 contained *OACT1* (*O*-acetyltransferase domain containing 1) and *E2F3* (E2F transcription factor 3), both known genes (Supplementary Table 2). It is not clear whether this region overlapped with the breakpoint region of the recurrent translocations t(6;19)(p22;q13) and t(6;9;22)(p22;q34;q11) in CML (Huret et al., 1989; Meza Espinoza et al., 2004; Yehuda et al., 1999), because the precise molecular breakpoints at 6p22 in these cases have not been characterized. The 346-kb region at 8p23.2 that showed copy number gain includes *CSMD1* (CUB and sushi multiple domains protein 1 precursor), the only transcriptome (Supplementary Table 2). Other abnormalities newly identified in this study involved mostly large regions of 2q26.2–q37.3 (16.8 Mb), 5q23.1–q23.3 (10.6 Mb), 5q31.2–q32 (6.50 Mb), 7p15.2–p14.3 (6.14 Mb), 7p21.3–p11.2 (41.7 Mb), 7q31.1-q31.33 (17.9 Mb), 8p21.3 (2.18 Mb), and 19p13.2–p12 (12.1 Mb), which made it difficult to pinpoint the candidate target genes.

DISCUSSION

In this article, we have shown genomewide detection of DNA copy number changes in a total of 55 CML patients at different stages using high-resolution array CGH. Using this technique, we delineated not only previously reported abnormalities, but also novel alterations involving narrow regions that may harbor only one or several candidate genes involved in the pathogenesis or disease progression of CML.

A number of cryptic copy number alterations that had been missed by karyotyping analysis were detected in array CGH analysis. Seven patients were found to have extra Ph chromosomes, which was the most frequent alteration in our series, although this alteration had not been detected by prior G-banding analysis in four of the seven patients (57%). In addition, more than 10 novel, cryptic copy number alterations were uncovered at a significantly higher frequency in patients in BC and AP, suggesting that these regions may contain genes relevant to the pathogenesis of CML, especially in progressive stages. Considering the wide variety of copy number alterations detected in AP/BC cases and that the majority of these abnormalities were observed in a single patient in our series, there might be a large heterogeneity in the molecular pathogenesis of CML AP/BC cases, and it may be possible that analysis of a larger number of patients could disclose novel recurrent molecular defects in CML. Alternatively, the genes included in the affected regions may also be deregulated by other mechanisms such as point mutations or epigenetic effects, which could not be detected by copy number analysis.

Many of the cryptic gains or losses affecting a single BAC locus are thought to represent copy number polymorphisms or LCVs rather than tumor-specific changes, and given their high frequency, it would be difficult to discriminate tumor-specific changes from LCVs. In our analysis, SBCs (or LCVs) seemed to be more frequently found in CML than in normal individuals using the same reference set (55 of 75 in CML vs. 3 of 10 in normal individuals, $P = 0.021$). Although

recent reports suggested a possible association of some LCVs with the regions implicated in cancer development (Iafrate et al., 2004; Sebat et al., 2004), the precise role of the LCVs detected in the current analysis in the pathogenesis of CML is still unclear and should be addressed in future studies that would include a larger number of normal subjects.

Although array CGH analysis successfully unveiled cryptic genomic aberrations in CML, we should note that it also has limitations in that the tumor content of the samples clearly affected the sensitivity of detecting copy number changes in tumor components. According to our admixture experiments, in which mixed tumor and normal DNA were tested for detection of a trisomy, the threshold of tumor content for detection of trisomies in our array CGH was estimated to be more than 20%–40% tumor components (data not shown). Thus, the trisomy 8 in AP3 and the monosomy 21 in AP4 as revealed by G-banding analysis were not expected to be detected in array CGH analysis because abnormal metaphases were found in only 2 of 20 with AP3 and 5 of 20 with AP4 (Tables 1 and 2). On the other hand, array CGH failed to detect the loss of chromosome 21 found in 17 of 20 metaphases in G-banding analysis in BC26, which was most likely a result of karyotypic overrepresentation of one or more rapidly proliferating tumor subclones in G-banding analysis. Finally, the FISH Mapped Clones V1.3 collection distributed from BACPAC Resources Center, which we used for array construction, does not cover some regions of particular interest in CML pathogenesis. For example, deletions of the 5′ region of the *ABL/BCR* junction on the der(9) chromosome, which is known to affect 10%–15% of the CML patients (Storlazzi et al., 2002), were missed in this study because our Human 1M arrays did not contain BAC clones including the *ABL* gene or the upstream *ASS* gene.

In conclusion, our array CGH analysis disclosed not only common chromosomal abnormalities, but also small, cryptic copy number alterations in CML genomes that were not detected by conventional analysis. It enabled a better description of genetic alterations in CML, which potentially could be applicable to molecular diagnostics and prediction of disease prognosis of this neoplastic disorder. The submicroscopic copy number alterations detected in this study might contribute to the identification of novel molecular targets implicated in the pathogenesis or disease progression of CML. Further studies with whole-genome tiling arrays having much higher resolutions will help to detect precisely the genes involved in the disease progression of CML.

ACKNOWLEDGMENTS

We are grateful to the late professor Hisamaru Hirai (Department of Hematology and Oncology, University of Tokyo) for his encouragement in this work. We dedicate this paper to his memory. We also thank Ms. Yasuko Ogino and Mr. Kenjirou Masuda (Lab Company Limited, Tokyo, Japan) for their technical assistance.

REFERENCES

Ahuja H, Bar-Eli M, Advani SH, Benchimol S, Cline MJ. 1989. Alterations in the p53 gene and the clonal evolution of the blast crisis of chronic myelocytic leukemia. Proc Natl Acad Sci USA 86:6783–6787.

Albertson DG, Pinkel D. 2003. Genomic microarrays in human genetic disease and cancer. Hum Mol Genet 12 Spec No 2:R145–R152.

Alimena G, De Cuia MR, Diverio D, Gastaldi R, Nanni M. 1987. The karyotype of blastic crisis. Cancer Genet Cytogenet 26:39–50.

Beck Z, Kiss A, Toth FD, Szabo J, Bacsi A, Balogh E, Borbely A, Telek B, Kovacs E, Olah E, Rak K. 2000. Alterations of P53 and RB genes and the evolution of the accelerated phase of chronic myeloid leukemia. Leuk Lymphoma 38:587–597.

Blick M, Romero P, Talpaz M, Kurzrock R, Shtalrid M, Andersson B, Trujillo J, Beran M, Gutterman J. 1987. Molecular characteristics of chronic myelogenous leukemia in blast crisis. Cancer Genet Cytogenet 27:349–356.

Calabretta B, Perrotti D. 2004. The biology of CML blast crisis. Blood 103:4010–4022.

Feinstein E, Cimino G, Gale RP, Alimena G, Berthier R, Kishi K, Goldman J, Zaccaria A, Berrebi A, Canaani E. 1991. p53 in chronic myelogenous leukemia in acute phase. Proc Natl Acad Sci USA 88:6293–6297.

Fiegler H, Carr P, Douglas EJ, Burford DC, Hunt S, Scott CE, Smith J, Vetrie D, Gorman P, Tomlinson IP, Carter NP. 2003. DNA microarrays for comparative genomic hybridization based on DOP-PCR amplification of BAC and PAC clones. Genes Chromosomes Cancer 36:361–374.

Fioretos T, Strombeck B, Sandberg T, Johansson B, Billstrom R, Borg A, Nilsson PG, Van Den Berghe H, Hagemeijer A, Mitelman F, Hoglund M. 1999. Isochromosome 17q in blast crisis of chronic myeloid leukemia and in other hematologic malignancies is the result of clustered breakpoints in 17p11 and is not associated with coding TP53 mutations. Blood 94:225–232.

Huret JL, Schoenwald M, Brizard A, Guilhot F, Vilmer E, Tanzer J. 1989. Chromosome 6p rearrangements appear to be secondary changes in various haematological malignancies. Leuk Res 13:819–824.

Iafrate AJ, Feuk L, Rivera MN, Listewnik ML, Donahoe PK, Qi Y, Scherer SW, Lee C. 2004. Detection of large-scale variation in the human genome. Nat Genet 36:949–951.

Kelman Z, Prokocimer M, Peller S, Kahn Y, Rechavi G, Manor Y, Cohen A, Rotter V. 1989. Rearrangements in the p53 gene in Philadelphia chromosome positive chronic myelogenous leukemia. Blood 74:2318–2324.

LeMaistre A, Lee MS, Talpaz M, Kantarjian HM, Freireich EJ, Deisseroth AB, Trujillo JM, Stass SA. 1989. Ras oncogene mutations are rare late stage events in chronic myelogenous leukemia. Blood 73:889–891.

Melo JV, Hughes TP, Apperley JF. 2003. Chronic myeloid leukemia. Hematology (Am Soc Hematol Ed Prog):132–152.

Meza Espinoza JP, Judith Picos Cardenas V, Gutierrez-Angulo M, Gonzalez Garcia JR. 2004. Secondary chromosomal changes in 34 Philadelphia-chromosome-positive chronic myelocytic leukemia patients from the Mexican West. Cancer Genet Cytogenet 148: 166–169.

Mitani K, Ogawa S, Tanaka T, Miyoshi H, Kurokawa M, Mano H, Yazaki Y, Ohki M, Hirai H. 1994. Generation of the AML1-EVI-1 fusion gene in the t(3;21)(q26;q22) causes blastic crisis in chronic myelocytic leukemia. Embo J 13:504–510.

Nakai H, Misawa S. 1995. Chromosome 17 abnormalities and inactivation of the p53 gene in chronic myeloid leukemia and their prognostic significance. Leuk Lymphoma 19:213–221.

Nakai H, Misawa S, Taniwaki M, Horiike S, Takashima T, Seriu T, Nakagawa H, Fujii H, Shimazaki C, Maruo N and others. 1994. Prognostic significance of loss of a chromosome 17p and p53 gene mutations in blast crisis of chronic myelogenous leukaemia. Br J Haematol 87:425–427.

Nakai H, Misawa S, Toguchida J, Yandell DW, Ishizaki K. 1992. Frequent p53 gene mutations in blast crisis of chronic myelogenous leukemia, especially in myeloid crisis harboring loss of a chromosome 17p. Cancer Res 52:6588–6593.

Nakamura T, Largaespada DA, Lee MP, Johnson LA, Ohyashiki K, Toyama K, Chen SJ, Willman CL, Chen IM, Feinberg AP, Copeland NG, Jenkins NA, Shaughnessy JD Jr. 1996. Fusion of the nucleoporin gene NUP98 to HOXA9 by the chromosome translocation t(7;11)(p15;p15) in human myeloid leukaemia. Nat Genet 12:154–158.

Pinkel D, Segraves R, Sudar D, Clark S, Poole I, Kowbel D, Collins C, Kuo WL, Chen C, Zhai Y, Dairkee SH, Ljung BM, Gray JW, Albertson DG. 1998. High resolution analysis of DNA copy number variation using comparative genomic hybridization to microarrays. Nat Genet 20:207–211.

Prigogina EL, Fleischman EW, Volkova MA, Frenkel MA. 1978. Chromosome abnormalities and clinical and morphologic manifestations of chronic myeloid leukemia. Hum Genet 41:143–156.

Rowley JD. 1973. Letter: A new consistent chromosomal abnormality in chronic myelogenous leukaemia identified by quinacrine fluorescence and Giemsa staining. Nature 243:290–293.

Sebat J, Lakshmi B, Troge J, Alexander J, Young J, Lundin P, Maner S, Massa H, Walker M, Chi M, Navin N, Lucito R, Healy J, Hicks J, Ye K, Reiner A, Gilliam TC, Trask B, Patterson N, Zetterberg A, Wigler M. Large-scale copy number polymorphism in the human genome. Science 305:525–528.

Sill H, Goldman JM, Cross NC. 1995. Homozygous deletions of the p16 tumor-suppressor gene are associated with lymphoid transformation of chronic myeloid leukemia. Blood 85:2013–2016.

Wang L, Ogawa S, Hangaishi A, Qiao Y, Hosoya N, Nanya Y, Ohyashiki K, Mizoguchi H, Hirai H. 2003. Molecular characterization of the recurrent unbalanced translocation der(1;7)(q10;p10). Blood 102:2597–2604.

Yehuda O, Abeliovich D, Ben-Neriah S, Sverdlin I, Cohen R, Varadi G, Orr R, Ashkenazi YJ, Heyd J, Lugassy G, Ben Yehuda D. 1999. Clinical implications of fluorescence in situ hybridization analysis in 13 chronic myeloid leukemia cases: Ph-negative and variant Ph-positive. Cancer Genet Cytogenet 114:100–107.

nature medicine

© 2006 Nature Publishing Group http://www.nature.com/naturemedicine

Thymus-derived leukemia-lymphoma in mice transgenic for the Tax gene of human T-lymphotropic virus type I

Hideki Hasegawa[1,2,8], Hirofumi Sawa[3,4,8], Martha J Lewis[2,5], Yasuko Orba[3], Noreen Sheehy[2], Yoshie Yamamoto[6], Takeshi Ichinohe[1], Yasuko Tsunetsugu-Yokota[7], Harutaka Katano[1], Hidehiro Takahashi[1], Junichiro Matsuda[6], Tetsutaro Sata[1], Takeshi Kurata[1], Kazuo Nagashima[3] & William W Hall[2]

Adult T-cell leukemia-lymphoma (ATLL) is a group of T-cell malignancies caused by infection with human T-lymphotropic virus type I (HTLV-I). Although the pathogenesis of ATLL remains incompletely understood, the viral regulatory protein Tax is centrally involved in cellular transformation. Here we describe the generation of HTLV-I Tax transgenic mice using the Lck proximal promoter to restrict transgene expression to developing thymocytes. After prolonged latency periods, transgenic mice developed diffuse large-cell lymphomas and leukemia with clinical, pathological and immunological features characteristic of acute ATLL. Transgenic mice were functionally immunocompromised and they developed opportunistic infections. Fulminant disease also developed rapidly in SCID mice after engraftment of lymphomatous cells from transgenic mice. Flow cytometry showed that the cells were $CD4^-$ and $CD8^-$, but $CD44^+$, $CD25^+$ and cytoplasmic $CD3^+$. This phenotype is indicative of a thymus-derived pre–T-cell phenotype, and disease development was associated with the constitutive activation of NF-κB. Our model accurately reproduces human disease and will provide a tool for analysis of the molecular events in transformation and for the development of new therapeutics.

HTLV-I infection is endemic in a number of well-defined geographical regions and it is estimated that as many as 20 million individuals are infected worldwide[1]. Although the vast majority of infected individuals remain clinically asymptomatic, some 2–5% will develop ATLL, which is a group of mature T-cell malignancies with distinct clinical presentations[2]. ATLL generally occurs in individuals infected around the time of birth and presents after prolonged latency periods ranging from 20 to 60 years. This is consistent with an age-dependent accumulation of leukemogenic events[1]. Transformed cells in ATLL are generally $CD4^+$ T lymphocytes[2], although other, less common phenotypes have been observed. These include $CD4^-CD8^-$ (refs. 3–7), $CD8^+$ (ref. 8) and $CD4^+CD8^+$ transformed cells[9,10], which suggests that infection and transformation of distinct cell populations during thymic development is important in the pathogenesis of ATLL.

The distinct clinical subtypes of ATLL include the two indolent forms, smoldering and chronic, and the extremely aggressive forms, acute and lymphomatous[2,11]. Individuals with aggressive ATLL present with extensive lymphadenopathy, hepatosplenomegaly, visceral invasion and characteristic cutaneous infiltration by malignant cells. Acute ATLL is also characterized by an aggressive high-grade T-cell leukemia, with leukemic cells showing a characteristic morphology of abnormally enlarged and cleaved nuclei, which are termed 'flower cells.' In addition to being poorly responsive to treatment, individuals with ATLL are functionally immunocompromised and develop a range of opportunistic infections similar to those seen in individuals with AIDS, such as *Pneumocystis jiroveci* pneumonia[2,11].

Although the pathogenesis of ATLL remains incompletely understood, the viral regulatory protein Tax seems to have a central role[1,12,13]. Tax, an extremely pleiotropic protein, has been shown to transform primary lymphocytes. This transformation is related to the ability of Tax to dysregulate the transcription of genes involved in cellular proliferation, cell-cycle control and apoptosis. Tax is a potent transcriptional transactivator not only of viral but also of cellular gene expression. The protein physically interacts with a number of cellular transcription factors, which include components of the NF-κB–Rel signaling complex, and persistent and constitutive activation of NF-κB is central to the development and maintenance of the malignant phenotype in ATLL[12–14]. Activation of NF-κB by Tax results in upregulation of the expression of a large number of cellular genes involved in cell proliferation, including a number of cytokines and their corresponding receptor genes[1,12–15] and this is believed to contribute to the autonomous expansion of infected and transformed cell populations.

[1]Department of Pathology, National Institute of Infectious Diseases, 4-7-1 Gakuen, Musashimurayama-shi, Tokyo 208-0011, Japan. [2]Centre for Research in Infectious Diseases, School of Medicine & Medical Science, University College Dublin, Belfield, Dublin 4, Ireland. [3]Laboratory of Molecular & Cellular Pathology and [4]Department of Molecular Pathobiology, Hokkaido University Research Center for Zoonosis Control and 21st Century COE Program for Zoonosis Control, N18 W9, Kita-ku, Sapporo, 060-8638, Japan. [5]Division of Infectious Diseases, UCLA School of Medicine, 10833 Le Conte Avenue, CHS 37-121, Los Angeles, California 90095, USA. [6]National Institute of Biomedical Innovation, Ibaraki-shi, Osaka 567-0085, Japan. [7]Department of Immunology, National Institute of Infectious Diseases, 1-23-1 Toyama, Shinjuku-ku, Tokyo 162-8640, Japan. [8]These authors contributed equally to this work. Correspondence should be addressed to W.W.H. (william.hall@ucd.ie).

Received 11 August 2005; accepted 5 December 2005; published online 19 March 2006; doi:10.1038/nm1389

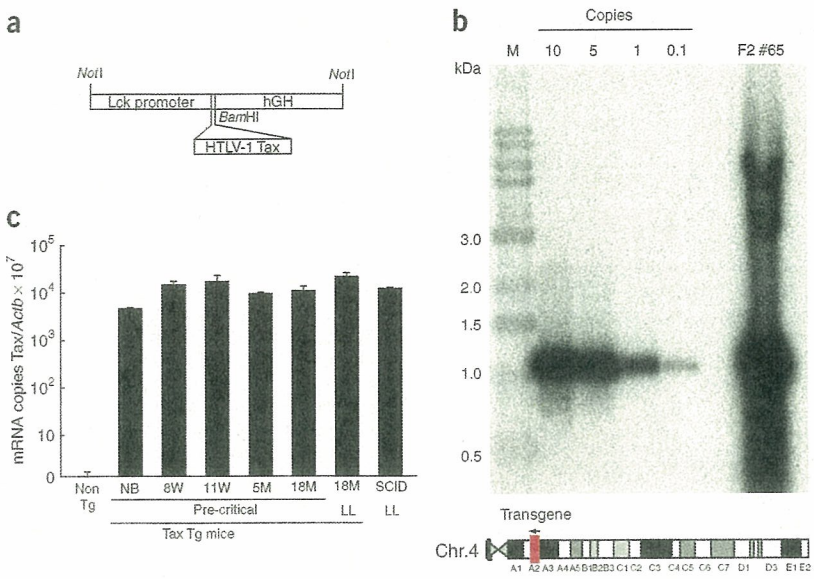

Figure 1 Construction of the Tax transgene and Tax mRNA expression in transgenic mice. (**a**) Schematic representation of the Tax transgene. HTLV-1 Tax cDNA was inserted in the *Bam*HI site of the p1017 vector at the 3′ end of the *Lck* proximal promoter. (**b**) Estimation of integrated Tax copy number and mapping of the Tax integration site (transgenic mouse #65) by chromosomal walking analysis. Tax copy numbers were investigated by Southern blot analysis of *Bam*HI-digested genomic DNA from the transgenic mouse (#65) in parallel with a serially diluted plasmid containing HTLV-I Tax cDNA. (**c**) Expression of Tax mRNA in Tax transgenic mice and SCID mice. RT-PCR was carried out on mRNAs extracted from spleens of newborn mice (NB), transgenic mice (Tg) at 8 weeks (8w), 11 weeks (11w), 5 months (5m), 18 months (18m), all without disease; 18 months with leukemia-lymphoma (18m LL) and in SCID mice with fulminant disease (SCID LL).

Attempts to directly show the oncogenic potential of Tax *in vivo* have been for the most part restricted to studies on expression of Tax in transgenic mouse models. These studies have resulted in a wide range of phenotypes, which have included the development of arthropathies, exocrinopathies, mesenchymal tumors, neurofibromas and large granular lymphocytic leukemia, a malignancy of natural killer cells[16–21]. None of the models, however, has developed T-cell lymphoma or leukemia identical to ATLL. To address this discrepancy, we have generated transgenic mice with expression of Tax restricted to developing thymocytes, and we have shown that after prolonged latency periods these mice develop lymphoma and leukemia with the clinical, pathological and immunological features characteristic of human disease.

RESULTS

Lymphoma and leukemia in HTLV-1 Tax transgenic mice

We generated transgenic mice expressing Tax under the control of the Lck proximal promoter, which restricts expression to developing thymocytes[22,23] because infection and transformation of cells during thymic development seems to be important in the pathogenesis of the disorder (**Fig. 1a**). We obtained three founder mice for each of the three lineages (#53, #14 and #17) and although each of the lineages was cross-bred with transgene-negative littermates, offspring were obtained from only one founder (#53; **Table 1**). PCR and Southern blot analysis of all founders and the progeny mice confirmed that all progeny carried the transgene. We studied transgene copy numbers and integration sites in selected mice. This number ranged from 10 to >20 copies, and genome walking analysis showed that the transgenes were tandemly inserted and integrated in the A2 region at position 14783143 of chromosome 4, which is a non-encoding region (**Fig. 1b**).

Gross pathological examination of Tax founder mice #14 and #17 killed at 23 months, and of all selected offspring from founder #53 ($n = 9$) beginning at 10 months, showed the development of marked splenomegaly, hepatomegaly, lymphadenopathy and the presence of large mesenteric tumors (**Fig. 2a,b** and **Table 1**). Hepatosplenomegaly was characteristically a 5–20-fold increase in organ size (**Fig. 2a–c**). Lymphadenopathy

Table 1 Establishment of HTLV-I Tax transgenic mice

Founder	F1	F2	Gender	Killed (month)	Involvement	Leukemia
#53	#50		M	12	Liver, spleen, bone marrow	+
	#52		M	17	Liver, spleen, kidney, lymph nodes, lung, skin, bone marrow, thymus	+
		#11	M	11	Early killing	–
		#12	F	14 (dead)	Liver, spleen, kidney, lymph nodes, lung, skin	ND
		#20	F	12 (dead)	Thymus[a]	ND
		#22	F	10	Liver, spleen, kidney, lymph nodes, lung, skin, eyelid, meninges, bone marrow	+
		#33	M	10	Early killing	–
		#36	F	18	Liver, spleen, lymph nodes, lung, bone marrow, thymus	–
		#44	F	19 (dead)	Liver, spleen, lymph nodes, lung	ND
		#52	F	17	Early killing	–
		#65	M	8	Early killing	–
#14			M	23	Liver, spleen, kidney, lymph nodes, lung, skin	+
#17			F	23	Liver, spleen, kidney, lymph nodes, lung, skin	+

Offspring were generated from one of three founder mice (#53). Three mice (#11, #52, #65) were killed before the development of disease (early death). One mouse (#20) unexpectedly died. The remaining mice were killed at the time points indicated. Gross lymphomatous involvement was as noted and all tissues were subjected to histological examination. Peripheral blood smears were examined for leukemic cells using Giemsa staining. M, male; F, female; ND, not determined.
[a]Thymus was exclusively examined; other organs were not examined.

© 2006 Nature Publishing Group http://www.nature.com/naturemedicine

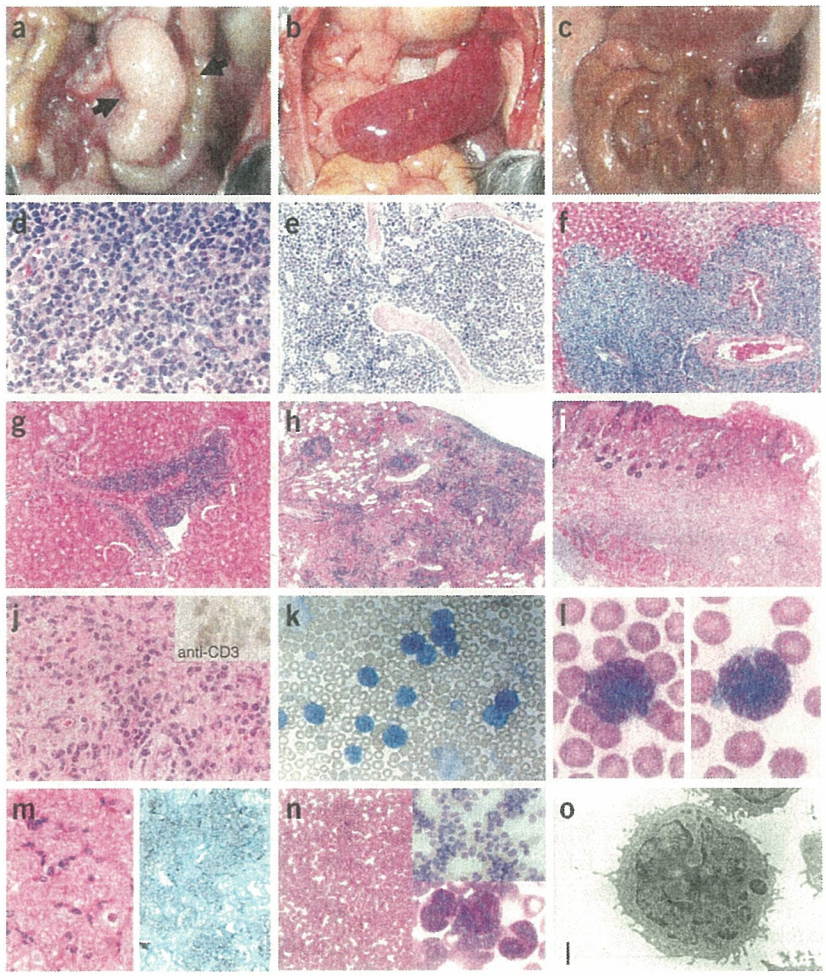

Figure 2 Pathological findings of T-cell lymphoma and leukemia in Tax transgenic mice. (**a**) Mesenteric tumor (black arrows) in the abdominal cavity of transgenic mouse #52. (**b**) Marked splenomegaly in transgenic mouse #22 with a greater than fivefold increase in size compared to an age-matched control littermate. (**c**) No tumors, lymphadenopathy or splenomegaly were evident in the control mice. Histological findings using H&E staining showed diffuse large-cell lymphoma in mesenteric lymph node (**d**), bone marrow with complete replacement of the marrow by lymphomatous cells (**e**), liver (**f**), kidney (**g**), lung (**h**) and lymphomatous infiltration of the skin with associated ulceration (**i**). (**j**) H&E staining and immunohistochemical staining with positive CD3-specific antibody staining (insert) of lymphomatous cells in the skin. (**k,l**) Peripheral blood smears from transgenic mouse #22. Leukemic cells with large and cleaved nuclei morphologically identical to flower cells found in human disease were present in peripheral blood smears of five mice. (**m**) H&E and Grocott staining of the lung showing opportunistic infection with *P. jiroveci*. (**n**) Peripheral blood smear with a large number of leukemia cells with segmented nuclei in a SCID mouse at 28 d after intraperitoneal injection of splenic lymphomatous cells from a transgenic mouse (lower magnification, left upper panel; higher magnification, left lower panel). Blood smear of a control age-matched SCID mouse is shown in the left panel. (**o**) Electron microscopic examination of leukemic cells from ascites fluid of SCID mice (original magnification, ×6,000). Cells showed enlarged cerebriform nuclei with disrupted chromatin and scanty cytoplasms typical of human ATLL cells. Scale bar, 500 nm.

© 2006 Nature Publishing Group http://www.nature.com/naturemedicine

was most often observed in the mesenteric, cervical and axillary lymph nodes but, in several cases, inguinal nodes were also involved. The mesenteric tumors ranged in size from 0.5 to 2.5 cm. All nine transgenic mice examined developed pathology beginning at 10 months of age, and findings were evenly distributed between males and females (**Table 1**). Histological examination showed diffuse, large-cell lymphomas involving spleen, lymph nodes, liver, thymus, bone marrow, kidney, lung, meninges and skin (**Fig. 2** and **Table 1**). Specifically, perivascular infiltration of lymphomatous cells was readily observed in the liver, kidney and lungs (**Fig. 2f–h**) and in mice with liver involvement; it seems likely that the cells had spread from the mesentery to the liver through the portal vein (**Fig. 2f**). Four mice examined had bone marrow involvement (**Fig. 2e**) with complete replacement of the marrow by lymphomatous cells. We documented involvement of the meninges in one mouse, but there was no evidence of invasion of the central nervous system parenchyma. Five of seven mice had cutaneous involvement with gross ulceration of the skin, and histologically had prominent infiltration of leukemic cells into the dermis, which is characteristic of ATLL. Immunohistochemical staining indicated that these cells expressed CD3 but not B220, showing that they were T-cell lymphomas (**Fig. 2j**). Overall, the histopathological findings are identical to those observed in ATLL, and the cytological characteristics of the lymphomatous cells are consistent with an aggressive malignancy and with the myriad of chromosomal abnormalities found in the disease[13].

Giemsa staining of peripheral blood smears in five mice showed the presence of large and abnormal leukemic cells with cleaved nuclei, which were morphologically identical to the flower cells observed in ATLL (**Fig. 2k,l**).

We also examined age- and sex-matched transgene-negative littermates in parallel for each mouse. We did not detect lymphoma in any of the nontransgenic littermates; however, two littermates that died from unknown causes did not have any abnormal gross or microscopic pathology. Three mice were killed before the development of disease, but there was no evidence of leukemia or lymphoma (**Table 1**). In addition to the development of leukemia and lymphoma, we found that transgenic mice were clinically immunocompromised. Mice with disease, but not control mice housed under identical conditions, developed severe pulmonary infections with *P. jiroveci* (**Fig. 2m**), which is characteristic of human ATLL.

Transfer of leukemia and lymphoma to immunodeficient mice

To develop a more consistent and rapid model of disease development and to facilitate immunological analyses, we attempted to induce leukemia and lymphoma in mice with severe combined immunodeficiency (SCID) after intraperitoneal and intradermal injection of lymphomatous spleen cells from individual transgenic mice. After

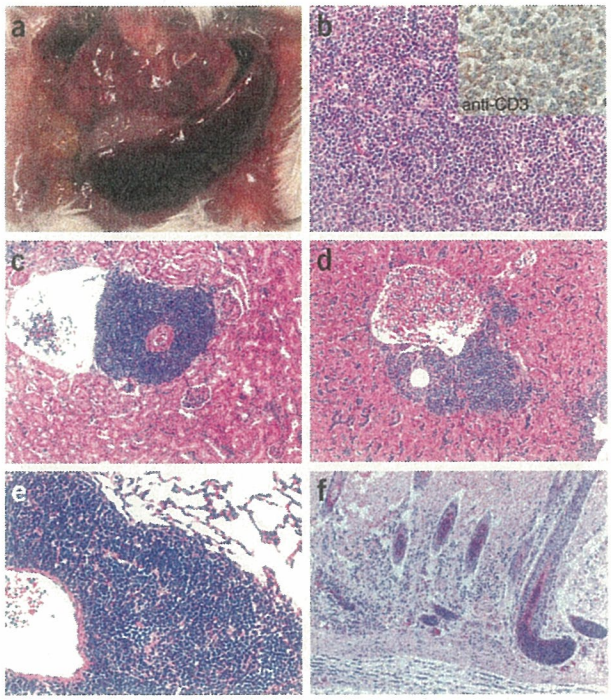

Figure 3 Gross and histological findings of lymphoma in SCID mice at 28 d after intradermal injection of lymphomatous cells from Tax transgenic mice. (**a**) Gross splenomegaly. Histological findings in spleen (**b**; insert, immunostaining showing positive staining for CD3-specific antibody), liver (**c**), kidney (**d**), lung (**e**) and skin (**f**). All organs showed extensive lymphomatous invasion.

© 2006 Nature Publishing Group http://www.nature.com/naturemedicine

direct transfer of cells from three transgenic mice, all SCID mice died within 28 d, having developed both an extremely aggressive leukemia with characteristic flower cells (**Fig. 2m**) and extensive lymphomatous involvement of the spleen, lymph nodes, bone marrow, liver, kidney and lung, which was identical to that observed in the original transgenic mice (**Fig. 3**). Notably, cutaneous involvement was only observed in those mice into which cells had been transferred by intradermal injection. Transmission electron microscopy of leukemic cells recovered from ascites fluid from SCID mice showed grossly enlarged and segmented cerebriform nuclei with markedly thin and scanty cytoplasms and a loss of polarity similar to that reported for ATLL and Sezary syndrome (**Fig. 2o**).

Flow cytometry analysis

We used flow cytometry to characterize the cell populations in both transgenic and SCID mice. Cells from transgenic spleens showed marked size heterogeneity with considerably higher forward scatter and side scatter compared to cells derived from spleens of control mice (**Fig. 4a**). Immunostaining of cells from SCID mice showed these were a distinct population and had a $CD3^-CD4^-CD8^-CD34^-c\text{-}kit^-$ phenotype (**Fig. 4b,c**). Staining for B-cell markers (B220) and macrophage markers (Mac 1) was negative (data not shown). Further analysis of SCID mice showed that the cells were $CD44^+CD25^+$ (**Fig. 4c**) and positive for cytoplasmic but not surface CD3 in both flow cytometric and immunofluorescence studies (**Fig. 4d,e**), all of which is consistent with a pre–T-cell, double-negative phenotype (**Fig. 4f**). A characteristic feature of ATLL is overexpression of CD25 (also known as IL-2 receptor α) on the surface of the transformed cells, and it is believed that Tax-mediated upregulation of both interleukin (IL)-2 and the IL-2 receptor has a major role in the autonomous proliferation of the transformed cell populations[14]. We examined the expression of CD25 in splenic lymphoma cells, and although the expression levels varied between tumor cells from different mice, a marked increase in expression was always evident (**Fig. 4d**). In addition, the T-cell activation marker CD69 was also found to be expressed at high levels on the lymphomatous cells (**Fig. 4d**).

NF-κB activation in transgenic and SCID mice

As it is well established that activation of NF-κB by Tax has a crucial role in transformation of cells by HTLV-I and in the maintenance of the malignant phenotype[12–14], we examined activity of NF-κB using both electrophoretic mobility shift assays (EMSAs) and enzyme-linked immunosorbent assays (ELISAs). EMSAs on nuclear extracts from transgenic splenic lymphoma cells showed marked NF-κB activity (**Fig. 5**) similar to that in a Epstein-Barr virus–transformed lymphoblastoid cell line used as a positive control. In contrast, no activity was evident in cells from normal mice (**Fig. 5a**). In addition, supershift assays (**Fig. 5b**) showed supershifted bands in the presence of antibodies for p50 and c-Rel, suggesting that formation of the p50–c-Rel complex is involved in the development and maintenance of the malignant phenotype (**Fig. 5b**). Evaluation of lymphomatous cells from SCID mice also confirmed activation of NF-κB. In contrast to the case of transgenic mice, this activation was found to involve only c-rel (**Supplementary Fig. 1** online). We also examined SCID mice by ELISA for activation of CREB, which was shown to be absent (**Supplementary Fig. 1** online).

Expression of Tax in transgenic mice

We used RT-PCR analysis of RNAs from splenic tissues to determine whether development of disease in both transgenic and SCID mice was associated with active expression of Tax (**Fig. 1c**). Although expression levels were low (10^4 less than expression of *Actb*, which encodes β-actin), Tax mRNA could be readily detected in newborn, asymptomatic, early-killed mice and in both transgenic and SCID mice with overt disease.

DISCUSSION

Here we showed that Tax expression alone in transgenic mice is sufficient to initiate the development of T-cell lymphoma and leukemia with clinical, pathological and immunological features similar or identical to those observed in ATLL. Specifically, the disorder in mice occurs after prolonged latency periods ranging from 10 to 23 months, which would be equivalent to the 20–60 years observed in human disease. The long time period before the onset of disease in the transgenic mouse model is also consistent with a multistep process of transformation. The clinical and pathological features of the disease were identical to those observed in the aggressive forms of ATLL, with widespread organ invasion by lymphomatous cells and the development of leukemia. Notably, the leukemia displayed the typical appearance of flower cells characteristic of ATLL, and these cells also had the expected morphological features when examined by electron microscopy.

ATLL has prominent cutaneous involvement, and this was reproduced in the transgenic model. Transgenic mice were also clinically immunocompromised and developed pulmonary infections with *P. jiroveci*, which is also characteristic of ATLL. The development of disease in transgenic mice and after transfer of disease to SCID mice was associated with activation of NF-κB, which is also found in ATLL.

© 2006 Nature Publishing Group http://www.nature.com/naturemedicine

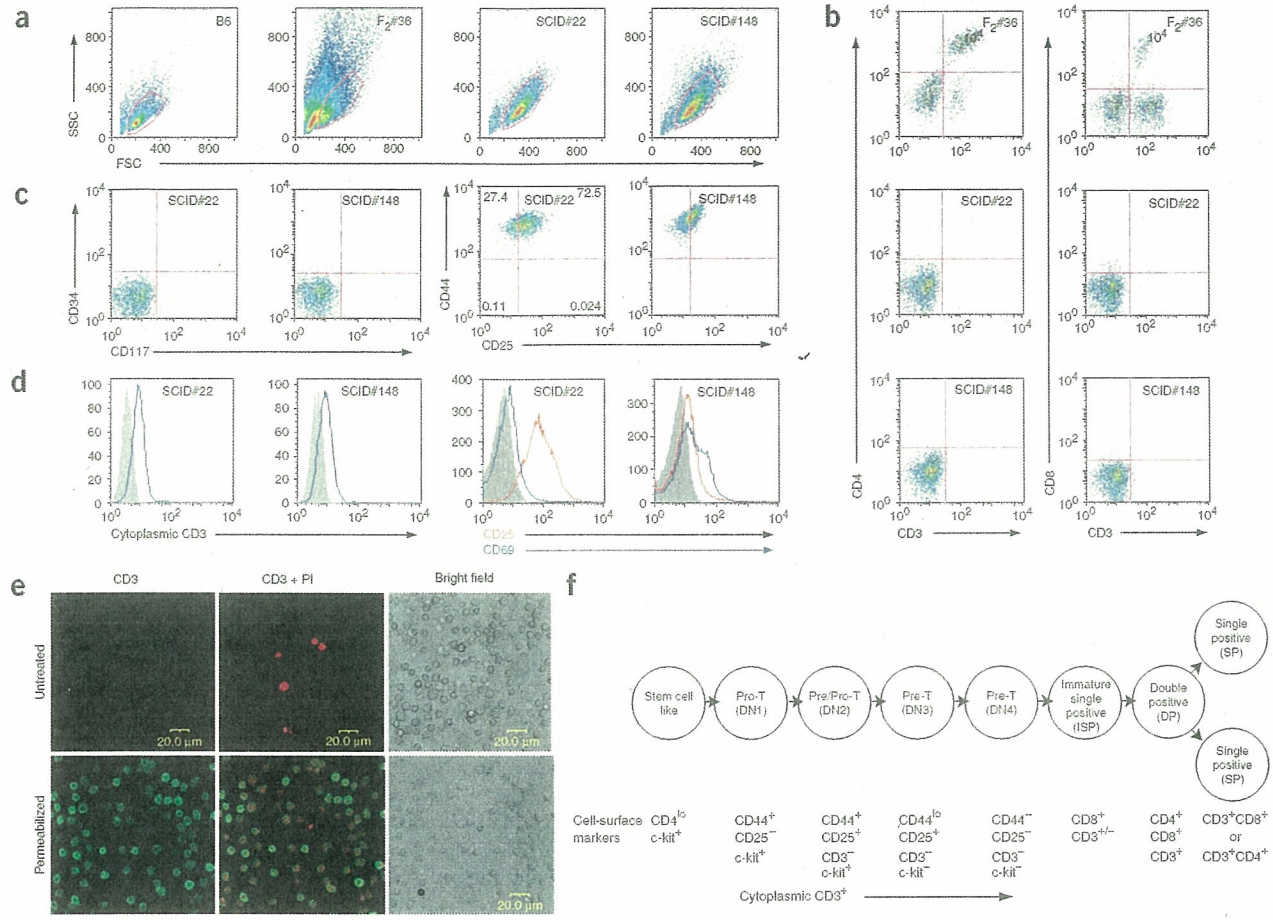

Figure 4 Flow cytometry analysis of cell-surface and intracellular markers in lymphomatous cells. We analyzed spleen-cell suspensions from transgenic mice with leukemia-lymphoma (#36), littermate control mouse (B6) and two SCID mice (#22, #148) with overt disease. (**a**) Forward-scatter (FSC) and side-scatter (SSC) analysis. (**b**) Expression of cell-surface markers CD3, CD4 and CD8. (**c**) Expression of cell-surface markers CD34, CD117 (also known as c-kit), CD44 and CD25. (**d**) Expression of CD25, CD69 and cytoplasmic CD3. (**e**) Surface and cytoplasmic CD3 staining of lymphomatous cells from SCID mice (SCID #22) with fulminant disease. Immunofluorescence studies show an absence of CD3 surface staining (untreated) but consistent and uniform cytoplasmic staining in permeabilized cells. Staining of nuclei using propidium iodide (PI) is indicated. (**f**) Schematic representation of T-cell development and corresponding immunological markers in the mouse thymus.

In the transgenic mice, this involved both the p50 and c-rel components, whereas after transfer to SCID mice, only c-rel seemed to be involved. The reasons for this are unclear, but such differences have also been observed in individuals with ATLL[24].

The malignant phenotype observed in the transgenic mice was a $CD4^-CD8^-$ double negative. Flow cytometric analysis also showed that transformed cells were $CD44^+$ and $c\text{-}kit^-$. Although surface staining for CD3 was negative, cytoplasmic CD3 staining was readily shown, and overall the cell markers were consistent with a thymic pre–T-cell phenotype[25,26]. The most common presenting phenotype in ATLL is $CD4^+$; however, there have been numerous reports describing the $CD4^-CD8^-$ phenotype in a considerable number of individuals with ATLL[3–7]. The different phenotypes observed in ATLL may well reflect the temporal relationships between infection with expression of Tax and the cell populations present at different stages of thymic development. It is likely that infection in most cases of human disease occurs after birth and much later than in our model. We are currently exploring the possibility of modifying the Lck promoters to allow control of Tax expression at different stages of thymic development to assess whether this will result in different phenotypes. It seems highly probable that use of the Lck promoter, which restricts expression of the transgene to developing thymocytes, has been crucial to the success of our mouse model. As noted previously, ATLL occurs after vertical transmission and is specifically associated with a history of breastfeeding. In rat models, intravenous or intraperitoneal inoculation of HTLV-I–infected cell lines results in considerable humoral and cellular immune responses. In contrast, these are absent after oral inoculation, and this hyporesponsiveness seems to contribute to successful infection[27]. Thus, both oral tolerance and the tropism of the virus for infection of developing T lymphocytes seem to be two key factors in the development of ATLL.

One major difference between our model and human disease is expression of Tax. Expression of Tax is rarely detected in ATLL, and this circumstance is thought to result primarily from highly efficient Tax-specific cellular immune responses that can effectively eliminate Tax-expressing T lymphocytes. Such responses, however, would certainly not occur in either transgenic or SCID mice. It has also been suggested that the lack of Tax expression in ATLL may be the result of

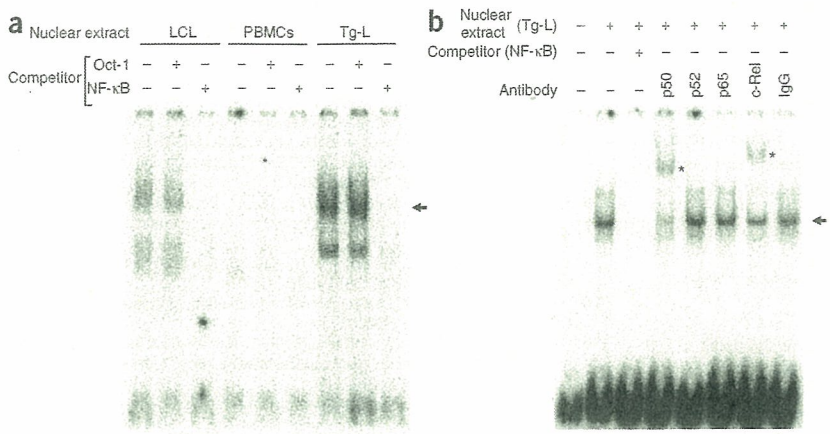

Figure 5 EMSAs showing activation of NF-κB in lymphomatous cells. (**a**) EMSAs of nuclear extracts from lymphomatous cells of transgenic mice and a positive control, the Epstein-Barr virus–transformed lymphoid cell line, and normal mouse PBMCs with a radiolabled NF-κB binding oligonucleotide probe. Specific shifted bands of NF-κB binding proteins (arrow) were exclusively detected in nuclear extracts from lymphoblastoid cell line and transgenic mice with disease (Tg-L) in the presence of the competitor. (**b**) Supershift assay of nuclear extracts from Tg-L using antibodies against p50, p65, p52, and c-Rel. Normal IgG was used as control. Supershifted bands were detected in extracts with p50-specific and c-Rel–specific antibodies.

© 2006 Nature Publishing Group http://www.nature.com/naturemedicine

epigenetic changes that restrict viral gene expression, but it is presently unclear whether such changes might at some point develop in this transgenic mouse model.

The models of ATLL developed in both transgenic and SCID mice will now allow detailed investigation of the role of Tax and the identification of specific molecular events associated with transformation. Moreover, the rapid development of fulminant disease in SCID mice will uniquely facilitate the evaluation of a range of therapeutic interventions that may ultimately lead to more effective treatments of human disease.

METHODS

Details are in **Supplementary Methods** online.

Mice. All mouse experimental protocols were approved by the Animal Care and Use Committee of the National Institute of Infectious Diseases, Tokyo, Japan, and by the Animal Research Ethics Committee of University College Dublin, Ireland. We purchased C57BL/6 mice from Charles River and the Oriental Yeast Company. We obtained SCID mice from Clea Japan.

Plasmid construction and generation of transgenic mice. We generated transgenic mice using inbred C57BL/6 mice and standard methods. We prepared the transgene construct (p*Lck*-Tax) by subcloning the HTLV-I Tax coding sequence into the *Bam*HI site of p1017 (provided by R.M. Perlmutter, University of Washington). We amplified Tax cDNA by PCR from DNA extracted from infected peripheral blood mononuclear cells (PBMCs). The p*Lck*-Tax plasmid was linearized by digestion with *Not*I (Boerhinger Mannheim), resulting in a 6.3-kb fragment containing the transgene, and this was purified using a Qiaex gel extraction kit (Qiagen) before injection. All mice were housed under specific pathogen-free conditions. Mice were killed after anesthesia with chloroform by syringe cardiac exsanguination. For detection of the transgene, we performed Southern blotting on genomic DNA extracted from tail-tip biopsies.

Chromosomal mapping of the inserted transgene. We identified genomic sequences flanking the transgenes by genomic walking methods[28] using the Universal Genome Walker kit (BD Bioscience Clontech) according to the manufacturer's instructions. Briefly, we constructed adaptor-ligated genomic DNA libraries of the transgenic mice using tail-tip DNA digested with four restriction enzymes: *Dra*I, *Pvu*II, *Eco*RV and *Stu*I; the genomic walk consisted of two PCR amplifications. We determined nucleotide sequences of PCR products by direct sequencing and identified specific chromosomal transgene insertion sites using BLAST searches of the flanking sequences in the Ensembl genome database.

Histopathological examination and immunohistochemistry. We directly fixed tissues in neutral-buffered formalin (Sigma), embedded them in paraffin, and sectioned and stained them with H&E. We stained additional sections with Grocott staining for detection of *P. jiroveci* cysts. We stained skin sections with CD3-specific antibody (Santa Cruz Biotechnology). We prepared peripheral blood smears using Giemsa staining and examined them with light microscopy.

Flow cytometry. We performed flow cytometry with a FACSCalibur (BD Bioscience Clontech) using standard methods. Briefly, we prepared single-cell suspensions from spleen in PBS containing 2% FCS and 0.05% sodium azide. For detection of surface antigens, we washed cells and stained them with saturating amounts of antibodies conjugated with FITC, PE or APC in the presence of blocking antibody 2.4G2 (FcR-specific) monoclonal antibody for 20 min on ice. For analysis of live cells, we added propidium iodide at a final concentration of 5 μg/ml. For detection of intracellular CD3, we stained cells with ethidium monoazide bromide (5 μg/ml), fixed them with 4% formaldehyde in PBS and incubated them in permeabilization buffer containing 0.5% saponin. We incubated cells with FITC-conjugated CD3-specific antibody or control monoclonal antibody (rat IgG2b). We carried out analysis using the Cell Quest program and reanalyzed data using FlowJo software (Tree Star) by gating live cells. Specific monoclonal antibodies used are detailed in **Supplementary Methods** online.

Immunofluorescence studies of surface and cytoplasmic CD3 staining. We collected cells (10^6) directly from spleen tissues from SCID mice, and washed and incubated them with CD3-specific antibody. Thereafter, we incubated samples with Alexa 488R–conjugated goat rabbit-specific IgG and then stained with propidium iodide (1 μg/ml). We permeabilized cells before incubation with primary antibody and detected immunofluorescent signals using a confocal microscope (IX70, Olympus).

EMSAs. We prepared nuclear extracts from 1–10 × 10^6 of lymphomatous cells from spleens of transgenic mice, an Epstein-Barr virus–transformed lymphoblastoid cell line, and PBMCs from control mice as previously described[29]. We performed an EMSA with the Gel Shift Assay Systems kit (Promega) according to the manufacturer's protocol. We separated samples by electrophoresis on 4% polyacrylamide gels in 0.25% Tris–boric acid–EDTA, and dried and analyzed them using a BAS 2000 image analyzer (Fujifilm).

Real-time quantitative PCR. We used real-time PCR (RT-PCR) to quantify expression of Tax mRNA in transgenic and SCID mice. We harvested spleens at birth and at 8 weeks, 11 weeks, 5 months, 18 months in transgenic mice without disease, and at 18 months in mice with leukemia-lymphoma, from control littermates and from SCID mice after intraperitoneal transfer of lymphomatous cells. We measured levels of Tax mRNA by RT-PCR after reverse transcription using the ABI PRISM 7900 sequence detection system (Applied Biosystems) with a QuantiTect Probe PCR kit (Qiagen).

Transfer of leukemia and lymphoma to SCID mice. We harvested spleen cells from transgenic mice and directly suspended them in RPMI medium. We directly injected cells (10^6) intraperitoneally or intradermally into SCID mice

from three individual transgenic animals. At 28 d, when mice were clearly ill, we carried out pathological and immunological studies as above.

Electron microscopy. We collected cells from ascites of SCID mice and fixed them in 2.5% glutaraldehye and 2% paraformaldehyde, postfixed them in 1% osmium tetroxide, dehydrated them and embedded them in epoxy resin. We stained ultrathin, 80-nm sections with uranyl and lead acetate and examined them with a JEM-1220 electron microscope (Jeol Datum) at 80 kV.

URL. Ensembl, http://www.ensembl.org

Note: Supplementary information is available on the Nature Medicine website.

ACKNOWLEDGMENTS

We thank Y. Sato and E. Tao for their technical assistance. We also thank O. Suzuki, T. Suzuki, M. Moriyama, K. Iwabuchi and Y. Misaki for advice. Y.O. is a Research Fellow of the Japanese Society for the Promotion of Science. These studies were supported by the Japanese Foundation for AIDS Prevention, Core Research for Evolutional Science and Technology (CREST), Ministry of Education and Culture, Japan and the National Virus Reference Laboratory, University College Dublin, Ireland.

COMPETING INTERESTS STATEMENT

The authors declare that they have no competing financial interests.

Published online at http://www.nature.com/naturemedicine/
Reprints and permissions information is available online at http://npg.nature.com/reprintsandpermissions/

1. Matsuoka, M. Human T-cell leukemia virus type I and adult T-cell leukemia. *Oncogene* **22**, 5131–5140 (2003).
2. Takatsuki, K. *et al.* Clinical diversity in adult T-cell leukemia-lymphoma. *Cancer Res.* **45**, 4644s–4645s (1985).
3. Hattori, T. *et al.* Leukaemia of novel gastrointestinal T-lymphocyte population infected with HTLV-I. *Lancet* **337**, 76–77 (1991).
4. Suzushima, H. *et al.* Double-negative (CD4- CD8-) T cells from adult T-cell leukemia patients also have poor expression of the T-cell receptor alpha beta/CD3 complex. *Blood* **81**, 1032–1039 (1993).
5. Kamihira, S. *et al.* Unusual morphological features of adult T-cell leukemia cells with aberrant immunophenotype. *Leuk. Lymphoma* **12**, 123–130 (1993).
6. Suzushima, H., Asou, N., Hattori, T. & Takatsuki, K. Adult T-cell leukemia derived from S100 beta positive double-negative (CD4- CD8-) T cells. *Leuk. Lymphoma* **13**, 257–262 (1994).
7. Shimauchi, T., Hirokawa, Y. & Tokura, Y. Purpuric adult T-cell leukaemia/lymphoma: expansion of unusual CD4/CD8 double-negative malignant T cells expressing CCR4 but bearing the cytotoxic molecule granzyme B. *Br. J. Dermatol.* **152**, 350–352 (2005).
8. Yamada, Y. *et al.* Adult T-cell leukemia with atypical surface phenotypes: clinical correlation. *J. Clin. Oncol.* **3**, 782–788 (1985).
9. Ohata, J. *et al.* CD4/CD8 double-positive adult T-cell leukemia with preceding cytomegaloviral gastroenterocolitis. *Int. J. Hematol.* **69**, 92–95 (1999).
10. Ciminale, V. *et al.* Unusual CD4+CD8+ phenotype in a Greek patient diagnosed with adult T-cell leukemia positive for human T-cell leukemia virus type I (HTLV-I). *Leuk. Res.* **24**, 353–358 (2000).
11. Uchiyama, T., Yodoi, J., Sagawa, K., Takatsuki, K. & Uchino, H. Adult T-cell leukemia: clinical and hematologic features of 16 cases. *Blood* **50**, 481–492 (1977).
12. Yoshida, M. Multiple viral strategies of HTLV-1 for dysregulation of cell growth control. *Annu. Rev. Immunol.* **19**, 475–496 (2001).
13. Jeang, K.T., Giam, C.Z., Majone, F. & Aboud, M. Life, death, and tax: role of HTLV-I oncoprotein in genetic instability and cellular transformation. *J. Biol. Chem.* **279**, 31991–31994 (2004).
14. Sun, S.C. & Yamaoka, S. Activation of NF-kappaB by HTLV-I and implications for cell transformation. *Oncogene* **24**, 5952–5964 (2005).
15. Hall, W.W. & Fujisawa, M. Deregulation of cell-signalling pathways in HTLV-I infection. *Oncogene* **24**, 5965–5975 (2005).
16. Nerenberg, M., Hinrichs, S.H., Reynolds, R.K., Khoury, G. & Jay, G. The tat gene of human T-lymphotropic virus type 1 induces mesenchymal tumors in transgenic mice. *Science* **237**, 1324–1329 (1987).
17. Hinrichs, S.H., Nerenberg, M., Reynolds, R.K., Khoury, G. & Jay, G. A transgenic mouse model for human neurofibromatosis. *Science* **237**, 1340–1343 (1987).
18. Green, J.E., Hinrichs, S.H., Vogel, J. & Jay, G. Exocrinopathy resembling Sjogren's syndrome in HTLV-1 tax transgenic mice. *Nature* **341**, 72–74 (1989).
19. Iwakura, Y. *et al.* Induction of inflammatory arthropathy resembling rheumatoid arthritis in mice transgenic for HTLV-I. *Science* **253**, 1026–1028 (1991).
20. Green, J.E., Baird, A.M., Hinrichs, S.H., Klintworth, G.K. & Jay, G. Adrenal medullary tumors and iris proliferation in a transgenic mouse model of neurofibromatosis. *Am. J. Pathol.* **140**, 1401–1410 (1992).
21. Grossman, W.J. *et al.* Development of leukemia in mice transgenic for the tax gene of human T-cell leukemia virus type I. *Proc. Natl. Acad. Sci. USA* **92**, 1057–1061 (1995).
22. Chaffin, K.E. *et al.* Dissection of thymocyte signaling pathways by *in vivo* expression of pertussis toxin ADP-ribosyltransferase. *EMBO J.* **9**, 3821–3829 (1990).
23. Wildin, R.S. *et al.* Developmental regulation of lck gene expression in T lymphocytes. *J. Exp. Med.* **173**, 383–393 (1991).
24. Mori, N. *et al.* Constitutive activation of NF-kappaB in primary adult T-cell leukemia cells. *Blood* **93**, 2360–2368 (1999).
25. Staal, F.J., Weerkamp, F., Langerak, A.W., Hendriks, R.W. & Clevers, H.C. Transcriptional control of T lymphocyte differentiation. *Stem Cells* **19**, 165–179 (2001).
26. Rezuke, W.N., Abernathy, E.C. & Tsongalis, G.J. Molecular diagnosis of B- and T-cell lymphomas: fundamental principles and clinical applications. *Clin. Chem.* **43**, 1814–1823 (1997).
27. Kannagi, M., Ohashi, T., Harashima, N., Hanabuchi, S. & Hasegawa, A. Immunological risks of adult T-cell leukemia at primary HTLV-I infection. *Trends Microbiol.* **12**, 346–352 (2004).
28. Noguchi, A. *et al.* Chromosomal mapping and zygosity check of transgenes based on flanking genome sequences determined by genomic walking. *Exp. Anim.* **53**, 103–111 (2004).
29. Dignam, J.D., Martin, P.L., Shastry, B.S. & Roeder, R.G. Eukaryotic gene transcription with purified components. *Methods Enzymol.* **101**, 582–598 (1983).

© 2006 Nature Publishing Group http://www.nature.com/naturemedicine